Quaternary Science Reviews 221 (2019) 105871

Contents lists available at ScienceDirect

Quaternary Science Reviews

journal homepage: www.elsevier.com/locate/quascirev

Mount Sedom salt diapir - Source for sulfate replenishment and gypsum supersaturation in the last glacial Dead Sea (Lake Lisan)

Elan J. Levy [a, b, *], Orit Sivan [a], Gilad Antler [a], Boaz Lazar [c], Mordechai Stein [b, c], Yossi Yechieli [b, d], Ittai Gavrieli [b]

[a] Department of Geological & Environmental Sciences, Ben-Gurion University of the Negev, Beer Sheva, 8410501, Israel
[b] Geological Survey of Israel, 32 Yesha'ayahu Leibowitz St., Jerusalem, 9692100, Israel
[c] Institute of Earth Sciences, The Hebrew University of Jerusalem, Givat Ram, Jerusalem, 91904, Israel
[d] Department of Hydrology and Microbiology, Zuckerberg Center, Ben-Gurion University of the Negev, Sede Boker, Israel

ARTICLE INFO

Article history:
Received 1 December 2018
Received in revised form
7 August 2019
Accepted 7 August 2019
Available online 23 August 2019

Keywords:
Pore-fluid
Sulfate isotopes
Last glacial
Dead sea
Lake Lisan
Mt. Sedom diapir

ABSTRACT

During the late Quaternary several hypersaline lakes occupied the tectonic depression of the Dead Sea Basin, depositing sequences of primary-evaporitic mineral phases: aragonite ($CaCO_3$), gypsum ($CaSO_4 \cdot 2H_2O$) and halite (NaCl). Aragonite and gypsum were the dominant primary mineral phases during the glacial periods and their formation required significant import of bicarbonate (HCO_3^-) and sulfate (SO_4^{2-}) ions to the lake. While bicarbonate was likely derived from dissolution of calcite in the watershed, the sources of sulfate remained elusive. Here we investigate and quantify the long-term sulfate reservoir changes in the deep waters (hypolimnion) of Lake Lisan (the last glacial Dead Sea) using concentrations and stable isotopes of sulfur in pore-fluids from the cores that were drilled at the lake floor (2010–11) by ICDP (International Continental Drilling Program). From ca. 117ka, pore-fluid sulfate concentrations increased and the brine attained supersaturation with respect to gypsum, peaking during the last glacial maximum (LGM; ca. 20ka). Stable isotopes of pore-fluid sulfate ($\delta^{34}S$ and $\delta^{18}O$) are similar to the values found in bulk sulfate minerals from the nearby Mount Sedom salt diapir. We suggest that relatively diluted and cool paleo-epilimnion water facilitated dissolution of halite and anhydrite ($CaSO_4$) of the Mt. Sedom salt diapir, resulting in a localized increase in solution density. Subsequently, this solution sank and mixed with saline hypolimnion water, simultaneously replenishing chloride, sodium and sulfate reservoirs, while diluting it with respect to other solutes. The mixing of the calcium-rich gypsum saturated hypolimnion and the sulfate-rich sinking brine from above resulted in gypsum supersaturation.

1. Introduction

Lake Lisan, the precursor of the modern Dead Sea during the last glacial period ca. 70-14 thousand years ago (ka), filled the tectonic depressions of the Dead Sea Basin and the Jordan Valley. At its highest stand, ca. 27ka to 23ka, with a lake level over 270 m (m) higher than today, it expanded over the area from Hazeva in the South to the Sea of Galilee in the North (Bartov et al., 2002; Begin et al., 1974, Neev and Emery, 1967; Haase-Schramm et al., 2004, Stein and Goldstein, 2017) (Fig. 1a). Its sheer size and lake level was determined by input of freshwater runoff from its 40 000 km^2 drainage basin (Stein et al., 1997), which was controlled mostly by the East Mediterranean–Levant hydroclimate (e.g. Stein, 2001, 2014; Torfstein et al., 2013). As a result of increasing freshwater runoff, a stable stratified (meromictic) configuration developed whereby a dense saline hypolimnion layer was capped by a less dense and saline epilimnion layer (Stein et al., 1997; Torfstein et al., 2005; Lazar et al., 2014).

The sedimentary record of Lake Lisan, termed the Lisan Formation (Fm.), is abundant with aragonite and gypsum, which are the primary evaporitic mineral phases, as well as silty detritus material (Katz et al., 1977; Stein et al., 1997; Haliva-Cohen et al., 2012). Similar to the Holocene Dead Sea, Lake Lisan was composed of calcium-chloride (Ca-Cl) brine characterized by excess calcium relative to sulfate and dissolved inorganic carbon species

* Corresponding author. Department of Geological & Environmental Sciences, Ben-Gurion University of the Negev, Beer Sheva, 8410501, Israel.
E-mail address: elanl@post.bgu.ac.il (E.J. Levy).

https://doi.org/10.1016/j.quascirev.2019.105871
0277-3791/

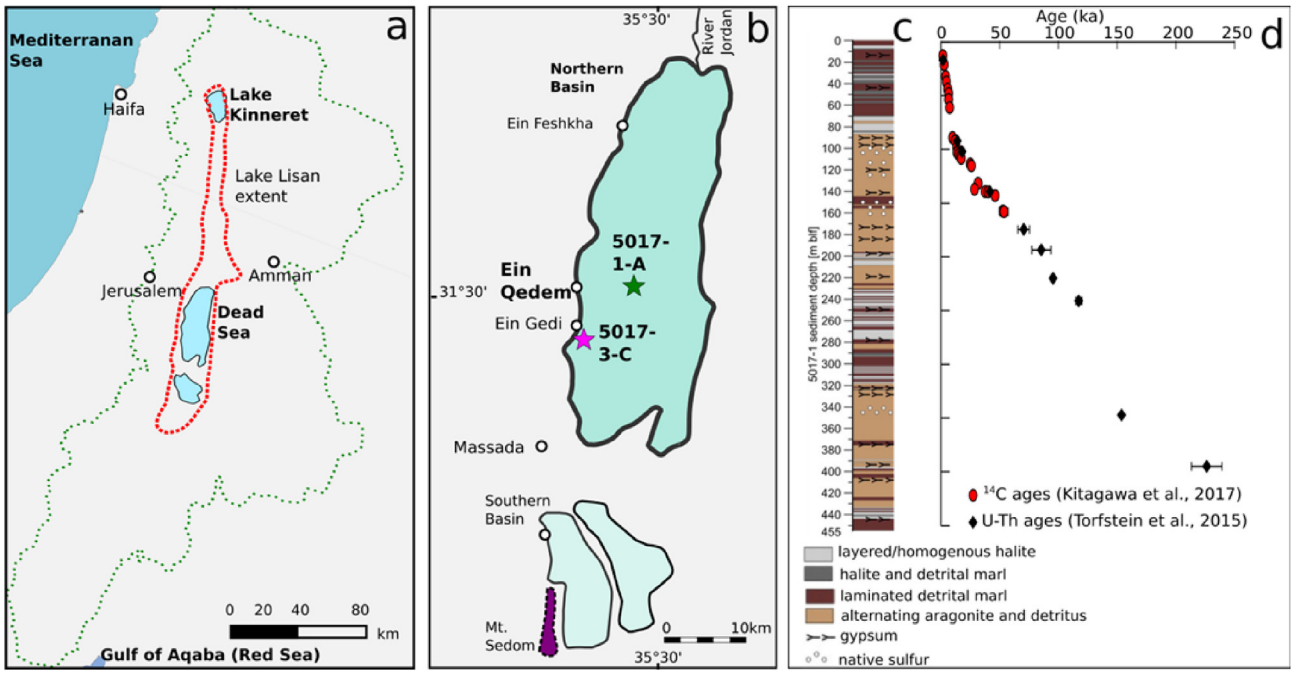

Fig. 1. The Dead Sea region, Lithological Section of core 5017-1-A and Ages. a- A regional map showing the modern Dead Sea, its watershed (marked by green dotted line) and the maximum extent of the last glacial Lake Lisan (red dotted line); **b-** The locations of Dead Sea cores 5017-1-A and 5017-3-C (green star and pink star, respectively) and Mt. Sedom salt diapir (purple); **c-** Composite lithology of core 5017-1-A (from Neugebauer et al., 2014); **d-** Radiocarbon ages of organic material (red circles) and U-Th ages from $CaCO_3$ (aragonite) (black squares). (For interpretation of the references to colour in this figure legend, the reader is referred to the Web version of this article.)

combined (mole $Ca^{2+} > SO_4^{2-} + HCO_3^- + CO_3^{2-}$), and chloride in excess of sodium (mole $Cl^- > Na^+$). The Ca-Cl brine's deficit in bicarbonate and sulfate required a supply of these ions to the lake from external sources to allow the deposition of aragonite and gypsum layers dominating the Lisan Fm. (Stein et al., 1997). It was suggested that dissolution of carbonates from Lake Lisan's watershed, including settled desert dust, by freshwater runoff, may have been the primary source of bicarbonate during that time (Belmaker et al., 2014). However, the origin of sulfate ions that allowed the precipitation of abundant gypsum layers in Lake Lisan and other lakes filling the Dead Sea Basin is less obvious (Torfstein et al., 2008; Torfstein and Turchyn, 2017).

Significant contributors of sulfate to the modern day Dead Sea are freshwater and saline springs (Starinsky, 1974; Stein et al., 1997; Torfstein et al., 2008). The upper Jordan River, which originates from the freshwater springs discharging at Mt. Hermon, as well as the Yarmouk River, Wadi Mujib, and Wadi Hasa could have provided sulfate to Lake Lisan (Torfstein et al., 2005). Additionally, freshwater runoff may also have derived sulfate from the dissolution of gypsic soils in the Lake Lisan's watershed (e.g. Palchan et al., 2019), though the extent of this sulfate source has yet to be addressed. A recent study by Weber et al. (2018) showed that the saline springs currently discharging to the Dead Sea most likely originate from Lake Lisan water. This finding raises a question whether the observed modern thermal saline springs found in and around the Dead Sea were active during the last glacial period. Indeed, in an earlier study, it was suggested that these types of Ca-Cl brines minimally contributed to the chemical budget of Lake Lisan (Stein et al., 1997).

Given the above sources of sulfate in freshwater inflow and assuming that saline springs were active during the last glacial period, it was estimated that sulfate could have accumulated in the epilimnion to the point of gypsum saturation (Torfstein et al., 2008). In order for thick (>10 cm) primary gypsum layers to have deposited, the hypolimnion must have also been saturated with respect to gypsum. To complicate matters Torfstein et al. (2005) showed that the Lisan Fm. gypsum carries an isotope signature ($\delta^{34}S$ and $\delta^{18}O$) which is characteristic of sulfate that underwent microbial sulfate reduction. During microbial sulfate reduction, sulfate concentrations are decreased which would result in a decrease of the degree of saturation with respect to gypsum, and thus the saturated solution would become undersaturated. It was suggested that microbial sulfate reduction occurred in the oxygen-depleted hypolimnion, a process that enriched the isotope composition of the residual sulfate in ^{34}S and ^{18}O, respectively. To compensate for decreasing sulfate concentrations a 'sulfur pump' mechanism was suggested; gypsum that precipitated from the epilimnion sank and dissolved in the hypolimnion, thereby replenishing its sulfate reservoir and keeping it at saturation with respect to gypsum. Periodic overturn and mixing between hypolimnion and epilimnion waters then produced the isotope enriched gypsum (Torfstein et al., 2005). This suggested 'sulfur pump' assumed that hypolimnion salinity and composition was similar to the present day Dead Sea, and given a high calcium concentration it could not have maintained high concentration of sulfate. While this model can explain the formation of isotope enriched gypsum in the Lisan Fm., it lacks direct evidence of the chemical composition Lake Lisan's hypolimnion.

The International Continental Drilling Program (ICDP) Dead Sea Deep Drilling Project (DSDDP) (2010–11) provides for the first time a window into the chemical composition of the hypolimnion (Lazar et al., 2014; Levy et al., 2017, 2018). Pore-fluids were extracted from the DSDDP 5017-1-A core that was drilled at the center of the lake at a water depth of 300 m where over 450 m of lake sediment spanning back ca. 220ka was recovered (Neugebauer et al., 2014; Torfstein et al., 2015, Kitagawa et al., 2017). The pore-fluids show that Lake Lisan's hypolimnion was significantly diluted relative to pore-fluids from the previous interglacial, and relative to present day Dead Sea. This is best evident by the drop in the concentration of magnesium (Mg^{2+}) and bromide (Br^-), which are considered to

be conservative elements in the system (i.e. the concentration changes in pore-fluids are equal to one another and, thus, do not reflect chemical processes that may have occurred in the lake or during early diagenesis). Indirect evidence for this dilution is by the concentration decrease of the non-conservative chloride (Cl^-) (Lazar et al., 2014), but this decrease is moderated, relative to Mg^{2+} and Br^-, due to halite dissolution (NaCl) (Levy et al., 2017). Based on Mg^{2+} and Br^- alone it was suggested that Lake Lisan reached a dilution factor of ~4 at its peak, in comparison to the modern Dead Sea (Levy et al., 2017). The increasing sodium chloride ratio (Na/Cl) in the pore-fluids in the Lisan Fm. suggests that dissolution of halite took place throughout most of the extended last glacial period (i.e. starting from ca. 117ka or marine isotope age [MIS] 5e). It was suggested that dissolution of rock salt at the Mt. Sedom salt diapir, found to the South-West of the modern Dead Sea (Fig. 1a), significantly replenished hypolimnion sodium and chloride inventories (Levy et al., 2018).

Using pore-fluid compositions we further investigate how Lake Lisan's hypolimnion composition changed. Given the suggestion that dissolution of the Sedom salt diapir played a significant role on sodium and chloride replenishment in Lake Lisan, we can also address the question whether dissolution of the salt diapir contributed to the lake sulfate budget. For this, we use the concentrations and stable isotopes of pore-fluid sulfate from the long ICDP cores, both at the deep and marginal sites of the Dead Sea, along with sulfate isotopes in minerals from Mt. Sedom. Based on the results we propose a conceptual model of solute fluxes from Mt. Sedom to Lake Lisan's hypolimnion, which can also explain the dilution of the hypolimnion under meromictic stratified conditions (Levy et al., 2017) and account for the thickness of the gypsum layers that were deposited intermittently in Lake Lisan.

1.1. Microbial sulfate reduction and gypsum precipitation in the modern Dead Sea

Both microbial sulfate reduction and gypsum precipitation were observed in the modern Dead Sea. Before the lake overturn in 1979 (Steinhorn, 1985), microbial sulfate reduction occurred in the anoxic hypolimnion layer of the lake (Nissenbaum and Kaplan, 1976). Massive gypsum precipitation occurred at the end of the 1950's and early 1960's as water level started to recede due to lowered freshwater input into the lake (Neev and Emery, 1967). Since then, both the gypsum precipitation potential and the sulfate to calcium ratio (SO_4^{2-}/Ca^{2+}) continuously decreased (Reznik et al., 2009). The small amount of gypsum that currently precipitates in the Dead Sea is masked by massive halite (NaCl) precipitation (Herut et al., 1998; Stiller et al., 1997; Gavrieli, 1997). Nevertheless, the saturation state of gypsum continued to rise and reached $\Omega = 1.4$ in 2009. The slow kinetics of gypsum nucleation which allows for this supersaturation may be explained by the low SO_4^{2-}/Ca^{2+} ratio in the brine (Reznik et al., 2009).

1.2. Mt. Sedom salt diapir

The Mt. Sedom salt diapir (the purple area in Fig. 1b), located at the south-west side of the Dead Sea basin, comprises a sedimentary section of around 2000m mostly comprising rock-salt (halite with some anhydrite; Fig. 2a). These sediments, termed the Sedom Fm. (Zak, 1967), originally deposited in the late Miocene to Pliocene Sedom lagoon which were then buried. During the Pleistocene, the rock-salt uplifted and breached through the overlying lacustrine sediments. Interaction with shallow ground water resulted in rock-salt dissolution (Vroman, 1950). This dissolution was suggested to have occurred by a Ca-Cl brine, saturated (or attaining saturation in the process) with respect to anhydrite/gypsum, which removed the halite components while leaving behind the less soluble anhydrite. Indeed it was suggested to have occurred at times when the lake transgressed over the western margins of the basin reaching the diapir (Zak, 1967). The widespread dissolution of the rock-salt formed a near horizontal salt mirror (green line in Fig. 2a), and a caprock of ~40 m thickness above, composed mostly of anhydrite and other insoluble sedimentary material (Zak, 1967, Fig. 2a). The roof of the caprock is an erosional surface on top of which are dotted remnants of parts of the Lisan Formation, implying that the diapir was submerged in the Lake Lisan water column.

2. Material and methods

2.1. Sampling

Details of the lithology of the DSDDP cores are reported in Neugebauer et al. (2014). Core 5017-1-A was drilled close to the middle of the modern lake (Fig. 1) at a water depth of ~300 m (~720 m below mean sea level = m bmsl). Core 5017-3-C was drilled off the shore of Ein Gedi Spa (Fig. 1) at water depth of ~2.5 m. The chronology of the 5017-1-A is given by Torfstein et al. (2015) and Kitagawa et al. (2017). The chronology of core 5017-3-C was constructed by lithological correlation to core 5017-1-A (Coianiz et al., 2019). Pore-fluid samples were collected during the drilling campaign of 2010/11 from core catchers and later in July 2012 at the GFZ -Potsdam from the core sections. Altogether 126 sediment samples of 15–30 ml in volume were extracted from core 5017–1–A and 46 samples from core 5017-3-C. Core catcher samples from both cores were taken in 50 ml plastic vials flushed with Ar gas. Pore-fluid was extracted by centrifugation and immediately purged with Ar gas. The core section samples were collected in 2013 into 50 ml plastic vials and sealed with nylon wrap. The upper 5 mm of sediment of these samples was removed before pore-fluid was extracted using a hydraulic press. All pore-fluid samples were subsequently filtered through a 0.45 μm syringe filter.

Twelve samples of bulk rock material weighing between 0.2 and 0.5 kg were collected from the evaporite outcrop of Sedom Fm. and its caprock (see Table 1). The samples were crushed, suspended in ~18 L of DDW and mixed intermittently over the course of 72 h, which allowed the complete dissolution of the soluble mineral phases (*i.e.* halite, anhydrite, gypsum). These solutions were subsequently filtered (0.45 μm).

2.2. Chemical and isotope analyses

Major cation concentrations were analyzed using ICP–AES at the Geological Survey of Israel (GSI). Bromide and chloride concentrations were analyzed by ICP–MS and titration at the GSI, respectively. Sulfate concentrations were measured by Dionex DX500 high-pressure liquid ion chromatography (HPLC) at Ben-Gurion University. Charge balance (i.e. reaction error) was always <5%.

Isotope analyses of sulfate were done on barite ($BaSO_4$) that was precipitated from the solution by adding saturated barium chloride ($BaCl_2$) solution. The barite was subsequently rinsed with acid and deionized water and set to dry in a 50 °C oven. The $\delta^{34}S_{SO4}$ and $\delta^{18}O_{SO4}$ values were determined at the Godwin Laboratory of the University of Cambridge. The barite precipitate was pyrolyzed at 1450 °C in a Temperature Conversion Element Analyzer (TC/EA), and the resulting carbon monoxide (CO) was measured by continuous flow GS-IRMS (Delta V Plus) for its $\delta^{18}O_{sulfate}$. For the $\delta^{34}S_{sulfate}$ analyses, the barite was combusted at 1030 °C in a Flash Element Analyzer (EA) and the resulting sulfur dioxide (SO_2) was measured with continuous flow GS-IRMS (Thermo, Delta V Plus). Samples for

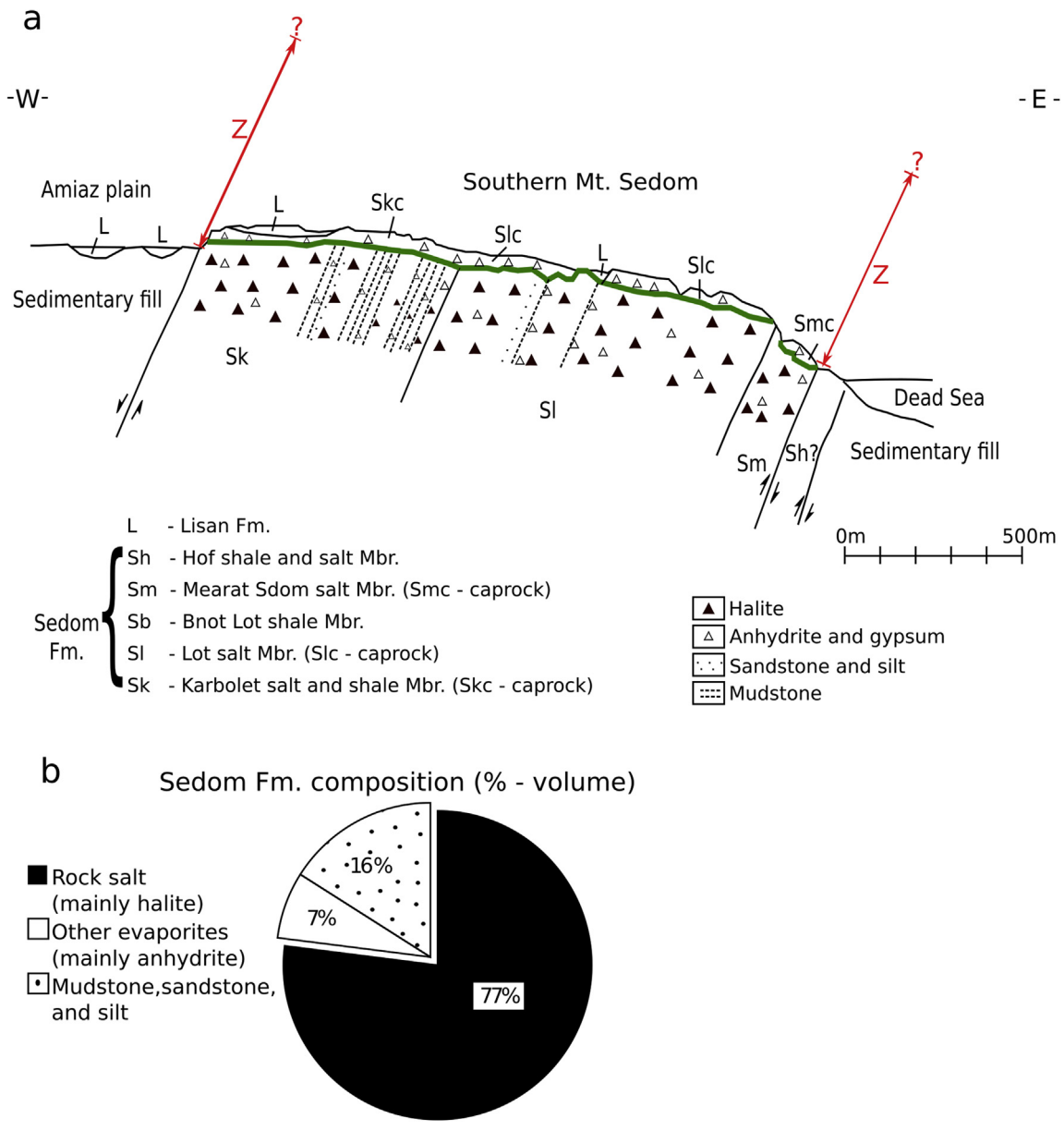

Fig. 2. A cross-section and composition of the Sedom salt diapir. a- A schematic cross section of the southern part of the Mt. Sedom diapir from Amiaz plain in the West to the Dead Sea in the East adapted from Weinberger et al. (1997) and lithology from Raab et al. (2000). The red double sided arrows labeled Z indicate the thickness of the missing diapir section which has been removed due to dissolution. The thick green line indicates the location of the dissolution surface or salt mirror. **b-** The general composition of the non-caprock component of the Sedom Fm. as estimated by Zak (1967) in pie chart display. (For interpretation of the references to colour in this figure legend, the reader is referred to the Web version of this article.)

Table 1
$\delta^{34}S_{bulk}$ and $\delta^{18}O_{bulk}$ of sulfate in bulk rocks of the Sedom Fm.

[a]	Sedom Fm. member:	Rock type:	Location	$\delta^{34}S$ (‰ -VCDT)	±	$\delta^{18}O$ (‰ SMOW)	±
1	Bnot Lot	Anhydrite	257284/554996	23.3	0.3	17.1	0.0
2	Karbolet	Caprock	236827/533639	19.1	0.3	17.7	0.5
3	Lot	Rock salt [a]	235819/550880	18.3	0.3	8.7	0.2
4	Lot	Rock salt	235695/559873	11.6	0.3	17.8	0.3
5	Lot	Caprock	235695/559873	13.4	0.3	18.7	0.6
6	Lot	Caprock	235802/560545	12.4	0.3	16.9	0.2
7	Lot	Rock salt	235802/560545	16.0	0.3	14.8	0.3
8	Lot	Caprock	235819/550880	16.1	0.3	17.8	0.8
9	Lot	Rock salt	235795/560549	17.7	0.3	12.0	0.9
10	Lot	Rock salt	235677/560270	18.4	0.3	7.8	0.7
11	Lot	Rock salt	237537/552664	17.2	0.3	12.8	0.3
12	Lot	Rock salt	235826/550882	17.8	0.3	13.1	0.8

[a] Rock salt is mostly consolidated halite but contains ~2.4% anhydrite based on averaged value from data in Raab et al. (2000).

$\delta^{18}O_{sulfate}$ were measured in replicates, and the standard deviation of analyses was used as the external reported error (~0.5‰). The $\delta^{18}O_{sulfate}$ values are reported vs. VSMOW and corrected for two barite standards of known $\delta^{18}O_{sulfate}$ that were run at the beginning and end of each set of samples (NBS 127 $\delta^{18}O_{sulfate} = 8.6$‰ and EM barite $\delta^{18}O_{sulfate} = 15$‰). $\delta^{34}S_{sulfate}$ results are reported vs. the Canyon Diablo Troilite (VCDT), and the error was determined using the standard deviation of the standard (NBS 127) at the beginning and the end of each run (±~0.4‰). The $\delta^{34}S_{sulfate}$ was also corrected to two standards of known sulfur isotope composition, NBS 127 (20.3‰) and EM barite (12‰). The presented $\delta^{34}S_{sulfate}$ and $\delta^{18}O_{sulfate}$ values of the pore-fluids are those in which sulfate concentrations were measured.

2.3. Saturation states and geochemical modeling

The saturation states for gypsum (Ω_{gypsum}); Eq. (1) in the pore-fluids were calculated using PHREEQC© applying the 'Pitzer' approach and Pitzer.dat data base (Pitzer, 1973; Parkhurst and Appelo, 1999; Reznik et al., 2009).

$$\Omega_{gypsum} = \frac{IAP}{K_{gypsum}} \quad (1)$$

where IAP and K_{gypsum} denote Ionic Activity Product and the gypsum solubility constant, respectively. Saturation states of anhydrite and halite ($\Omega_{anhydrite}$ and Ω_{halite}, respectively) were also calculated using PHREEQC©.

3. Results

Chloride (Cl^-), magnesium (Mg^{2+}) and calcium (Ca^{2+}) concentrations from pore-fluids extracted from the DSDDP 5017-1-A core show abundant variability over the entire core depth (Fig. 3a–c). Bromide (Br^-) shows similar trends to magnesium (Levy et al., 2017) which is evident by the uniform bromide to magnesium (Br^-/Mg^{2+}) ratio (pink circles in Fig. 3d). Due to this, both bromide and magnesium are regarded as conservative ions in the pore-fluids (Levy et al., 2017). Both ions are also considered highly conservative in the Dead Sea during evaporation until the precipitation of Carnallite ($KMgCl_3 \cdot 6H_2O$) (Zilberman et al., 2017). Over the entire core, the concentration trends of these conservative ions generally change trend-direction in sediment intervals containing halite as opposed to no halite in the core: increase in ion concentrations correlate occurs in intervals where halite layers are present as opposed to decreasing concentrations where they are not. Levy et al. (2017) modeled the subsurface transport to assess the effects of diffusion over time on conservative ion concentrations. The similarity between the measured pore-fluid concentrations (black diamonds in Fig. 3b for Mg^{2+}) and the estimated pre-diffusion concentrations (red dotted line in Fig. 3b) infers that subsurface diffusion of the pore-fluid solutes was mostly hampered, and that the long term chemical evolution at the sediment-water interface in the hypolimnion was retained in the pore-fluid. This retention was attributed to both the low permeability of sediments found in core 5017-1-A (i.e. fine detrital material and halite layers) and the relatively high viscosity of the pore-fluid solutions, both acting to lower the effective diffusion coefficients of solutes (Levy et al., 2017).

The depth interval of study is between 235 and 89mblf (meters below lake floor) or ca. 117ka to 11.5ka, between MIS 5e until the end of the Younger Dryas, as represented by the upper and lower boundaries of the black dotted lines in Fig. 3i to p. Long-term dilution trends of magnesium and calcium are evident along this interval (Fig. 3j and k). The ratio of calcium to magnesium (Ca^{2+}/Mg^{2+}) shows a general decrease from bottom-up over the entire core and highlights inventory change of calcium relative to the conservative magnesium (black diamonds in Fig. 3d). However, in the interval of study this ratio is mostly uniform (Fig. 3l). In comparison, the sulfate (SO_4^{2-}) shows clear increase within this interval (Fig. 3e and m). From 235mblf to 142mblf (ca. 117ka to 44ka), concentrations range between 3.4 mM and 8.9 mM before gradually increasing and reaching a maximum of 33 mM at 106mblf (ca. 20ka) and falling again in the depths directly above. The saturation state of gypsum, Ω_{gypsum} (Fig. 3f), follows the sulfate concentration trends but with values either near saturation ($\Omega_{gypsum} \approx 1$) or supersaturation ($\Omega_{gypsum} > 1$) between 235 and 142mblf (ca. 117ka to 44 ka) and then at a maximum value of $\Omega_{gypsum} = 3.3$ at 106mblf (20.2ka).

The general lithology of core 5017-1-A (Fig. 3: right of the pore-fluid profiles) indicates roughly where the primary gypsum layers are found in the core. Indeed Torfstein and Turchyn (2017) investigated the isotope composition of the primary gypsum layers (blue triangles in Fig. 3o and p). Neither chloride, magnesium, nor calcium concentrations (Fig. 3i, j, 3k) show any evidence suggesting significant compositional changes in these solutes coeval to the appearance of primary gypsum layers. However, sulfate concentrations (Fig. 3m) and the saturation state of gypsum (Fig. 3n) show secular decreases in values in pore-fluid samples at similar depths to the gypsum layers. The $\delta^{34}S_{sulfate}$ in the pore-fluids within the interval of study is between 11 and 22‰ (Fig. 3o) while the $\delta^{18}O_{sulfate}$ in the pore-fluids is between 9 and 17‰ (Fig. 3p). Both $\delta^{34}S_{sulfate}$ and $\delta^{18}O_{sulfate}$ (black diamonds) are equal to or lower than the $\delta^{34}S_{gypsum}$ and $\delta^{18}O_{gypsum}$ gypsum values found at similar stratigraphic intervals in the core (blue triangles). Unlike the $\delta^{34}S_{sulfate}$ and $\delta^{18}O_{sulfate}$, the $\delta^{34}S_{gypsum}$ and $\delta^{18}O_{gypsum}$ display an increasing trend over the interval corresponding to the Lisan Fm. (data from Torfstein and Turchyn, 2017). In pore-fluids from core 5017−3−C, drilled close to the Dead Sea shores, the $\delta^{34}S_{sulfate}$ range between −6.3–5.7‰ and $\delta^{18}O_{sulfate}$ between 13.1 and 16.3‰, respectively (Table A1 in appendix), i.e., lower $\delta^{34}S_{sulfate}$ than the corresponding values in core 5017-1-A. The $\delta^{34}S$ values from bulk rocks of the Sedom Fm. from Mt. Sedom (Table 1) range between 11.6 and 23.3‰, and $\delta^{18}O$ ranges between 7.8 and 18.7‰.

4. Discussion

4.1. General

Given that the pore-fluid magnesium concentrations are representative of hypolimnion concentrations, the long term decrease in sediments corresponding to ca. 117ka to 12.5ka was suggested to be the result of increasing freshwater runoff into the lake along with mixing of these diluted waters with hypolimnion brine (Levy et al., 2017; Lazar et al., 2014). Chloride concentrations (Fig. 3a and i) also decrease within this depth interval, however the magnitude of dilution of chloride is much less than that of magnesium. Levy et al. (2018) proposed that this relatively 'moderate' decrease was caused by an addition of chloride from the dissolution of halite at the Sedom salt diapir which counteracted the extent of dilution from freshwater. Halite dissolution is also evident in the increases in the sodium (Na^+) concentration and the Na/Cl ratio (Levy et al., 2018). An additional dramatic compositional change is shown by sulfate concentrations, which significantly increase in the same sediment interval. Below, we quantify, determine the source and investigate the mechanism leading to the obseved sulfate increase (i.e. did it occur in-situ in pore-fluids or is it representative of the hypolimnion), while also explaining the observed high supersaturation with respect to gypsum. We then synthesize the pore-fluid compositional data and propose a paleo-limnological model

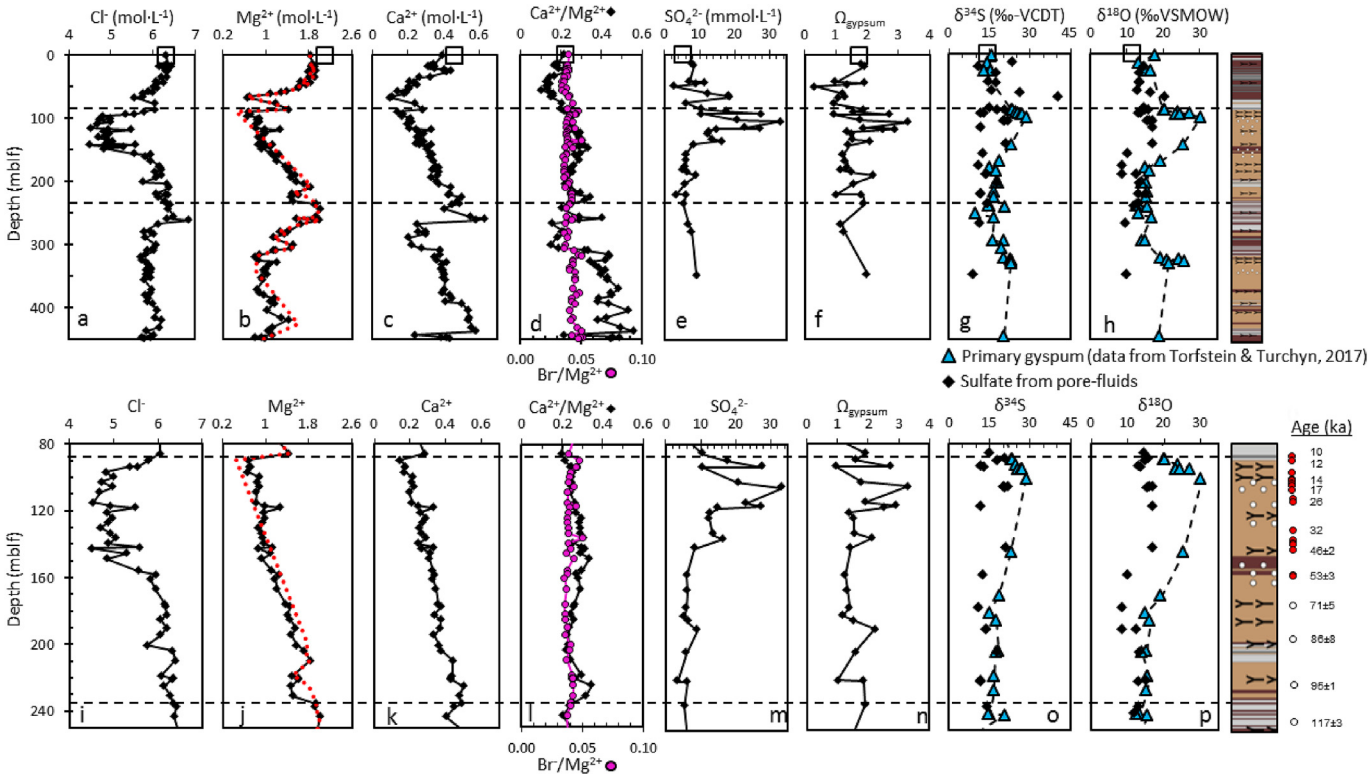

Fig. 3. Ion concentrations and isotope compositions of pore-fluid extracted from core 5017-1-A. a- Cl^-; **b-** Mg^{2+} (black diamonds) and the diffusion corrected Mg^{2+} (red dotted line) (Levy et al., 2017); **c-** Ca^{2+}; **d-** Ca^{2+}/Mg^{2+} concentration ratio (top axis; black diamonds) and comparative Br^-/Mg^{2+} ratio (bottom axis; pink circles); **e-** SO_4^{2-}; **f-** Ω_{gypsum}; **g-** $\delta^{34}S$ of sulfate in pore-fluids ($\delta^{34}S_{sulfate}$; black diamonds) and primary gypsum layers from the core ($\delta^{34}S_{gypsum}$; blue triangles); **h-** $\delta^{18}O_{SO4}$ (notations as in **g**). Figs. **i**, **j**, **k**, **l**, **m**, **n**, **o** and **p** are zoom-in of the area marked by the black dashed lines in Figs. **a** to **h**. The isotope data for gypsum layers presented in Figs. **g**, **h**, **o** and **p** are taken from Torfstein and Turchyn (2017). Composite lithology of 5017-1-A (Neugebauer et al., 2014), radiocarbon ages of organic material (red circles; Kitagawa et al., 2017) and U-Th ages from $CaCO_3$ (aragonite) (empty circles; Torfstein et al., 2015) are given on the right. The open squares are the Dead Sea values at 100 m water column depth from 2013. (For interpretation of the references to colour in this figure legend, the reader is referred to the Web version of this article.)

which can explain these changes.

4.2. Sulfate accumulation in Lisan Fm. Pore-fluids

Various processes may have led to the observed increase in sulfate in the hypolimnion of Lake Lisan, as recorded by the pore-fluids from the core. During the last glacial Lake Lisan, thick layers of primary gypsum precipitated from the lake, indicative of a lake containing a significant sulfate inventory (Torfstein et al., 2005, 2008). This primary gypsum is imprinted with increasing $\delta^{34}S_{gypsum}$ and $\delta^{18}O_{gypsum}$ values as a function of time (blue triangles in Fig. 3o and p), and was attributed to microbial sulfate reduction in the Lake Lisan's water column (Torfstein et al., 2005, 2008). The 'sulfur pump' mechanism (see Fig. 4 in Torfstein et al., 2005) describes a stable stratified configuration for Lake Lisan which is a requirement for long term microbial sulfate reduction in the hypolimnion. Sulfate in the epilimnion, derived from both freshwater and saline spring sources, accumulated, and precipitated periodically as gypsum to the hypolimnion. In the hypolimnion bacterial sulfate reduction consumed sulfate but in doing so it enabled dissolution of the precipitating gypsum from above. It was suggested that this process resulted in continuous replenishment of the hypolimnion sulfate reservoir and also allowed for $^{34}S_{sulfate}$ and $^{18}O_{sulfate}$ enrichment relative to the initial hypolimnion sulfate values. Upon partial or full overturn of the stratified lake, resulting from lake level drops, and mixing of the epilimnion $^{34}S_{sulfate}$ depleted and hypolimnion $^{34}S_{sulfate}$ enriched sulfate reservoirs, thick primary gypsum layers with relatively isotope enriched values deposited on the lake floor.

According to the 'sulfur pump' mechanism described above (Torfstein et al., 2005), the isotope composition of sulfate in the hypolimnion is expected to be at least equal to if not more enriched in comparison to the primary gypsum. The model further suggests that $\delta^{34}S_{sulfate}$ values in the hypolimnion will reach values as high as, or in excess of, ~40‰. However, the pore-fluid $\delta^{34}S_{sulfate}$ in Lisan Fm. is either equal to or lower than the values of gypsum at corresponding depth intervals (black diamonds in comparison to blue triangles in Fig. 3o and p). Additionally, the observed supersaturation with respect to gypsum in the pore-fluids cannot be explained by gypsum dissolution, since this process can only take place when the solution is undersaturated and will cease once saturation is attained. Thus, both the lower isotope values of the pore-fluid sulfate, and the supersaturation of the pore-fluids must be explained by a process different to the 'sulfur pump' mechanism.

To emphasize the magnitude of the sulfate reservoir replenishment and the importance of identifying its source, we revert to the maximum pore-fluid sulfate concentrations of 33 mmol L^{-1} (mM) and $\Omega_{gypsum} = 3.3$ found at 106mblf (ca. 20ka). At gypsum saturation ($\Omega_{gypsum} = 1$) the sulfate concentration in this pore-fluid would only be 12 mM (based on calculations in PHREEQC software). Thus, the pore-fluid contains an excess of 21 mM sulfate above saturation. If the original hypolimnion was saturated, then pore-fluid sulfate concentrations would have increased threefold, and the additional sulfate would have altered the original sulfate isotope signature.

Early diagenetic processes, such as microbial disproportionation

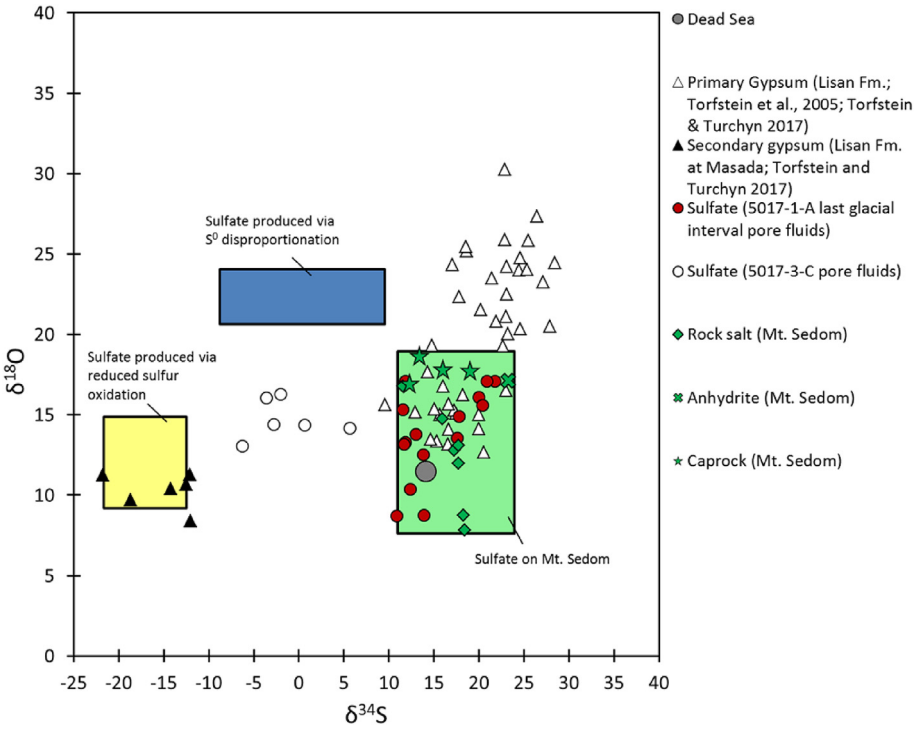

Fig. 4. Plot of $\delta^{34}S$ (‰; VCDT) vs. $\delta^{18}O$ (‰; VSMOW) of sulfate from various sources. Pore-fluids in the last glacial interval in core 5017-1-A (red filled circles), sulfate in core 5017-3-C (empty circles), primary gypsum layers from the Lisan Formation in core 5017-1-A and the lake margins (empty triangles; data from Torfstein et al., 2005; Torfstein and Turchyn, 2017), and secondary gypsum from the Lisan Formation found at Masada (black triangles, data from Torfstein and Turchyn, 2017). Also shown are sulfate minerals found within the caprock from Mt. Sedom (green stars), anhydrite layer (green cross) and disseminated sulfate within rock salt (green diamonds) of Mt. Sedom. Additionally, the range of sulfate values from Mt. Sedom (green rectangle) and the ranges for theoretical $\delta^{34}S_{sulfate}$ and $\delta^{18}O_{sulfate}$ as a result of sulfur disproportionation (blue rectangle), and as a result of oxidation of reduced sulfur minerals (yellow rectangle) are shown. (For interpretation of the references to colour in this figure legend, the reader is referred to the Web version of this article.)

of elemental sulfur (S^0), may contribute sulfate to the pore-fluid in-situ in the sediment (i.e. Thamdrup et al., 1993; Böttcher and Thamdrup, 2001; Böttcher et al., 2001, 2005). Yet as shown in Fig. 4, and explained below, the expected sulfate $\delta^{34}S$ and $\delta^{18}O$ isotopes produced from sulfur disproportionation and those found in the pore-fluid are dissimilar. There is a large S and O isotope fractionation associated with bacterial disproportionation of S^0. According to Böttcher et al. (2001), the sulfate produced is enriched in ^{18}O and ^{34}S by ~17.4‰ relative to the water, and by 11.0–18.4‰ relative to the S^0, respectively. Accordingly, $\delta^{18}O_{sulfate}$ in our profiles should be closer to the range of 20.5–24.0‰ given a $\delta^{18}O_{H2O}$ value of 4.5–6.5‰ in Lake Lisan (Lazar et al., 2014), and $\delta^{34}S_{sulfate}$ of −8.5–9.8‰ assuming $\delta^{34}S_S$ of −8.6 to −19.5‰ (Bishop et al., 2013; Torfstein et al., 2008). Given the expected isotope composition of the excess sulfate produced by disproportionation, this process is unlikely to be responsible for the observed sulfate isotope enrichment (blue rectangle in Fig. 4).

Oxidation of reduced sulfur, such as iron sulfide minerals (*i.e.* FeS_2), elemental sulfur (S^0) and volatile or dissolved sulfide (H_2S), may increase sulfate concentrations and alter the $\delta^{34}S_{sulfate}$ and $\delta^{18}O_{sulfate}$ composition. However, as in disproportionation, the expected $\delta^{34}S_{sulfate}$ and $\delta^{18}O_{sulfate}$ isotopes produced via oxidation of reduced sulfur (yellow rectangle in Fig. 4) cannot explain the observed sulfate isotope composition of the pore-fluid. The $\delta^{34}S_{sulfate}$ produced during oxidation would be in the range of −12.5‰ to −21.7‰, similar to that of the sulfide source, and the $\delta^{18}O_{sulfate}$ would be in the range of 9–15‰, assuming a combination of the solution H_2O (4.5‰ and 6.5‰; Lazar et al., 2014) and oxygen derived from the atmosphere (~+23‰) at a $\delta^{18}O_{H2O}$:$\delta^{18}O_{atm}$ ratio of 3:1 and 2:2, respectively (e.g., Balci et al., 2007; Calmels et al., 2007; Torfstein and Turchyn, 2017).

Sulfate from pore-fluid in core 5017-3-C, drilled close to the Western shore of the Dead Sea at Ein Gedi Spa (drilled at water depth of ~3 m), shows relatively lower $\delta^{34}S_{sulfate}$ values (empty circles in Fig. 4) in comparison to pore-fluid from core 5017-1-A (drilled at the deepest floor of the modern Dead Sea; red filled circles in Fig. 4). The $\delta^{34}S_{sulfate}$ values from the shallow site core 5017-3-C are closer to the isotope composition of secondary gypsum that was found at the exposures of the Lisan Fm. at marginal terraces such as those found at PZ1 section at Perazim Valley. It was suggested that the formation of this secondary gypsum was as a result of the oxidation of reduced sulfide by percolating meteoric water into the Lisan Fm. followed by gypsum precipitation (Torfstein et al., 2005; Torfstein and Turchyn, 2017). Thus, the sediments of core 5017-3-C may have been exposed to atmospheric/hydrological processes during the recent or geological past, similar to the process suggested at have occurred at the marginal terraces. To conclude, given that early diagenetic or epigenetic processes cannot explain the observed sulfate isotope signatures found in core 5017-1-A pore-fluid, we infer that the sulfate concentrations were not altered in the sub-surface and are representative of Lake Lisan's hypolimnion compositions. Thus, using these concentrations, it is possible to make first order estimations of sulfate reservoir replenishment in Lake Lisan.

4.3. Quantifying the lake sulfate reservoir replenishment

A first order estimate of the increase in lake sulfate inventory is carried out by using magnesium concentrations as a reference and assuming that its inventory remained constant (i.e. its concentration decrease reflects only dilution by freshwater), and that the water column was homogenous (see also Kiro et al., 2017; Levy

et al., 2018). The equation for the lake's volume at a particular time during the Lisan period is then given by (Eq. (2); adapted from Kiro et al., 2017 and Levy et al., 2018):

$$V_t = \frac{[Mg^{2+}]_0}{[Mg^{2+}]_t} \cdot V_0 \quad (2)$$

Where V_t and V_0 are the lake's volume at time t and at reference time 0, and $[Mg^{2+}]_0$ and $[Mg^{2+}]_t$ are the lake's magnesium concentrations at these times, respectively. The reference values used were the 2013 Dead Sea magnesium concentration (2.101 M; Levy et al., 2018) and Dead Sea volume (130 km^3) as calculated by the hypsometric curve (Hall, 1996) from the corresponding lake level (−428 m bmsl). The change in the inventory of any dissolved species S, ΔS, in the time interval $\Delta t = t_2 - t_1$ (where $t_2 \geq t_1$) is given by:

$$\Delta S = [S]_{t_2} \cdot V_{t_2} - [S]_{t_1} \cdot V_{t_1} \quad (3)$$

where the square brackets denote concentration. Substituting Eq. (3) into Eq. (2) yields the change in inventory of species S:

$$\Delta S = \left[Mg^{2+}\right]_0 \cdot V_0 \cdot \left(\frac{[S]_{t_2}}{[Mg^{2+}]_{t_2}} - \frac{[S]_{t_1}}{[Mg^{2+}]_{t_1}} \right) \quad (4)$$

Note that for a conservative species, Eq. (4) yields $\Delta S = 0$ (*i.e.* for conservative species S, $[Mg^{2+}]_0 \cdot V_0 = [Mg^{2+}]_{t_1} \cdot V_{t_1} = [Mg^{2+}]_{t_2} \cdot V_{t_2}$ and $[S]_{t_1} \cdot V_{t_1} = [S]_{t_2} \cdot V_{t_2}$).

According to Eq. (4), the increase in sulfate inventory of the lake, ΔSO_4^{2-}, was ~$9 \cdot 10^{12}$ mol during the time interval of $t_1 = 117$ka to $t_2 = 20$ka (core depth of 106mblf at sulfate peak concentrations). Based on the same equation at the same time interval, the chloride and sodium inventories also increased. The ΔCl^- increased by ~$6.3 \cdot 10^{14}$ mol, which represents a ~70% increase in the lake's chloride inventory, whereas the contemporaneous ΔNa^+ inventory increased by ~$6.5 \cdot 10^{14}$ mol (calculated using concentrations found in the DR material of Levy et al., 2017). Levy et al. (2018) suggested that the increase in chloride and Na/Cl ratio during the extended last glacial reflects dissolution of halite at the Mt. Sedom salt diapir. Additional evidence also showed similarities for the estimated rate of pore-fluid chloride accumulation in comparison to the rate of Mt. Sedom uplift and halite exposure. Furthermore, the increase in stable $\delta^{37}Cl$ values of the chloride was suggested to result from dissolution of halite at Mt. Sedom. The simultaneous increase in the inventories of chloride and sodium as well as that of sulfate during the Lisan period, although differing by 2 orders of magnitude, may infer that the solutes came from a common source and were supplied into the hypolimnion by the same mechanism over the studied time interval. In section 4.4 below, we quantify dissolution of the evaporites on Mt. Sedom and demonstrate its potential significance for reservoir replenishment of chloride, sodium and sulfate in Lake Lisan, with particular emphasis on sulfate.

4.4. Mt. Sedom as a source for sulfate in Lake Lisan

If indeed the dissolution of rock salt from Mt. Sedom provided chloride and sodium to Lake Lisan (Levy et al., 2018), then anhydrite and some gypsum, which are also present in the salt diapir, could have dissolved and supplied sulfate to the lake. However, it remains unclear whether enough sulfate deriving from Mt. Sedom could account for the observed reservoir replenishment in the hypolimnion as shown by pore-fluid compositions.

Zak (1967) suggested that the Sedom Fm. comprises ~77% rock salt, predominantly halite, with up to 2.4% (weight percent) of disseminated anhydrite, according to Raab et al. (2000). Ignoring the heterogeneous composition of rock salt and assuming that the addition of $6 \cdot 10^{14}$ mol chloride ($\Delta Cl_{inventory}$) between ca. 117ka to 20ka (see Section 4.2, Eq. (4)) resulted entirely from dissolution of Mt. Sedom rock salt, then the volume of rock salt which was dissolved can be estimated. This time interval of ca. 117 to 20ka is significant as pore-fluids show a mostly ongoing increase of the Na/Cl ratio, which suggests mostly continuous halite dissolution (Levy et al., 2018).

Given the surface area of Mt. Sedom (16 km^2), it is possible to estimate the thickness of the missing section of the diapir (Z in Fig. 2a) that was dissolved (Eq. (5)):

$$Z\,(m) = \frac{\Delta Cl_{\text{inventory}}\,(mol) \times M.W._{NaCl}\left(\frac{gr}{mol}\right) \times 1000\left(\frac{m}{Km}\right)}{\rho_{d-RS}\left(\frac{gr}{Km^3}\right) \times A\,(km^2) \times f_{RS}} \quad (5)$$

Where $\Delta Cl_{inventory}$ is the chloride inventory replenishment, $M.W._{NaCl}$- NaCl molecular weight of halite (58.4 gr·mol^{-1}), ρ_{d-RS}- bulk density of rock salt in Mt. Sedom (2.115 10^3 kg m^{-3}; Zak, 1967; Weinberger et al., 2006), A-surface area of the diapir (16 Km^2) and f_{RS} - fraction of rock salt in the Sedom Fm. (0.77; Zak, 1967). Inserting these values in Eq. (5) yields Z ~1300 m as the estimated missing section of the diapir from which the halite was derived.

The sulfate reservoir from anhydrite layers included within the same section of Mt. Sedom can now be estimated (Eq. (6)):

$$[SO_4]_{layered}(mol) = \frac{Z\,(Km) \times A\,(km^2) \times f_{CaSO4} \times \rho_{d-CaSO4}\left(\frac{Kg}{Km^3}\right)}{M.W._{CaSO4}\left(\frac{Kg}{mol}\right)} \quad (6)$$

Where $\rho_{d-CaSO4}$- density of anhydrite (2.97 10^3 kg m^{-3}), f_{CaSO4}- fraction of anhydrite in Sedom Fm. (0.07; assuming for a first order estimate that 7% of the diapir is anhydrite from Zak, 1967; Raab et al., 2000) and $M.W._{CaSO4}$- molecular weight of anhydrite (136.14 g mol^{-1}). Table 2, column 2 presents the calculated moles of sulfate in the anhydrite layers ($[SO_4]_{layered}$) as a function of the thickness of the missing section of Mt. Sedom diapir (Z).

An additional reservoir of sulfate in Mt. Sedom is found in disseminated form, mostly as anhydrite, within the rock salt, and comprises on average ~2.4% bulk weight (Raab et al., 2000). The potential contribution of this sulfate reservoir to the lake can be estimated from the mass of rock salt in Mt. Sedom that is assumed to have dissolved:

$$[SO_4]_{dissem}(mol) = \frac{Z\,(Km) \times A\,(km^2) \times f_{RS} \times \rho_{d-RS}\left(\frac{Kg}{Km^3}\right) \times fw_{SO4-RS}}{M.W._{SO4}\left(\frac{Kg}{mol}\right)} \quad (7)$$

Where fw_{SO4-RS} - the weight fraction of sulfate in the rock salt (0.024) and $M.W._{SO4}$ - the molecular weight of sulfate (96.1 gr·mol^{-1}). Table 2, column 3 presents the calculated moles of sulfate in the rock salt ($[SO_4]_{dissem}$) and in column 4 the total sulfate reservoir available (*i.e.* $[SO_4]_{layered} + [SO_4]_{dissem} = [SO_4]_{Total}$) as a function of the thickness of the missing section of Mt. Sedom diapir (Z). Some of this available sulfate must have been retained in the caprock in which the sulfate average weight proportion is 55% (Raab et al., 2000). The amount of sulfate in the caprock can be

Table 2
Sulfate reservoir estimates (mol) given estimated thicknesses of the missing section (Z) of the Mt. Sedom diapir which underwent dissolution. The caprock sulfate reservoir estimate is also shown (column 5). Note that in all cases the excess sulfate free to reach the Dead Sea is greater than the calculated replenishment ($\Delta SO_{4-inventory}$) of sulfate to the lake ($9\cdot10^{12}$ mol).

Thickness (Z) of Mt. Sedom exposed to dissolution	$[SO_4]_{layered}$ in mol (Eq. (6))	$[SO_4]_{dissem}$ in mol (Eq. (7))	$[SO_4]_{Total}$ in mol	$[SO_4]_{caprock}$ in mol (Eq. (8))	$[SO_4]_{Excess}$ in mol
1300 m (This study – maximum thickness)	$3.2\cdot10^{13}$	$8.5\cdot10^{12}$	$4.1\cdot10^{13}$	$7.0\cdot10^{12}$	$3.4\cdot10^{13}$
600 m (Zak and Bentor, 1972; Weinberger et al., 2006, 2007)	$1.5\cdot10^{13}$	$3.9\cdot10^{12}$	$1.9\cdot10^{13}$	$7.0\cdot10^{12}$	$1.2\cdot10^{13}$
800 m (Zak and Bentor, 1972; Weinberger et al., 2006, 2007)	$2.0\cdot10^{13}$	$5.2\cdot10^{12}$	$2.5\cdot10^{13}$	$7.0\cdot10^{12}$	$1.8\cdot10^{13}$

estimated:

$$[SO_4]_{caprock}(mol) = \frac{C(km) \times A(km^2) \times \rho_{d-CR}\left(\frac{Kg}{Km^3}\right) \times fw_{SO4-CR}}{M.W_{\cdot SO4}\left(\frac{Kg}{mol}\right)} \quad (8)$$

Where C- average thickness of the caprock (0.04 km), ρ_{d-CR}- bulk density of caprock ($1.92\cdot10^3$ kg m^{-3}; Zak, 1967) and fw_{SO4-CR} –average weight fraction of sulfate in the caprock (0.55; Raab et al., 2000). Solving Eq. (8) yields a caprock sulfate inventory of $7.0\cdot10^{12}$ mol.

Subtracting the caprock sulfate reservoir (column 5) from the total sulfate reservoir available (column 4), within the 1300 m thick missing section of Mt. Sedom leaves some $3.4\cdot10^{13}$ mol of sulfate that can contribute to replenishment of the Lake Lisan hypolimnion ($[SO_4]_{Excess}$; column 6). This value is greater than the calculated change in the sulfate inventory ($\Delta SO_{4-inventory}$) in the lake from pore-fluids ($9\cdot10^{12}$ mol, section 4). Given these assumptions, the Mt. Sedom sulfate reservoir from dissolution of a 1300 m thick missing section, is more than sufficient to account for the observed increase of sulfate in pore-fluids.

The estimated thickness of the missing dissolved section (Z) of 1300 m on Mt. Sedom is based on the assumption that it is the sole source for replenishment of the chloride reservoir in Lake Lisan. This estimate is greater than the 600 m–800 m values suggested by Zak and Bentor (1972), which were estimated from the thickness of the caprock. Indeed, Levy et al. (2018) suggested that Mt. Sedom was not the only source of halite dissolved, and some halite, which precipitated during the preceding last interglacial period, was also dissolved. Yet, even when considering the lower estimates of 600 m–800 m of dissolved missing section in Mt Sedom, the sulfate reservoirs within them can still account for both the sulfate content found in the caprock and the observed sulfate increase as shown by pore-fluids.

Another important line of evidence attesting to Mt. Sedom being a dominant source for sulfate in Lake Lisan comes from sulfate isotope compositions. An overlap of pore-fluid $\delta^{34}S_{sulfate}$ and $\delta^{18}O_{sulfate}$ values and isotopes from anhydrite layers, disseminated sulfate within the rock salt and the caprock on Mt. Sedom exists (Fig. 4). This suggests that Mt. Sedom contributed sulfate directly to Lake Lisan and required no complex pathways or isotope fractionation.

4.5. Model for dilution and compositional changes of Lake Lisan hypolimnion

The chemical composition of Lake Lisan's hypolimnion, as derived from the pore-fluid records of core 5017-1-A, shows dilution of conservative magnesium and bromide as well as chloride, and is evidence for mixing with diluted epilimnic waters (Lazar et al., 2014; Levy et al., 2018). Information about the epilimnion composition may be inferred from the saline brine that is currently discharging at the Western shores of the Dead Sea (Fig. 1b). Weber et al. (2018) suggested that the Ca-Cl brine solution discharging to the modern Dead Sea by the Ein Qedem saline springs dating to ca. 20 to 40ka comprises diluted Lake Lisan epilimnion which penetrated the Judean Mountain Aquifer during a period of high lake stand. In comparison to the relatively high Na/Cl ratio in the Lisan Fm. pore-fluid from similar time intervals, the Ein Qedem brine, which discharges into the Dead Sea 50 km North of Mt. Sedom, is characterized by low Na/Cl ratio, suggesting that the lake's upper waters, were less impacted by the dissolution of the rock salt.

A conceptual model hypothesizing the paleo-limnological conditions in Lake Lisan can be made which is based on: 1) Dissolution of the major evaporites on Mt. Sedom by the epilimnion solution of Lake Lisan, followed by: 2) gravity-driven transport of the cascading solute-loaded epilimnion solution from Mt. Sedom to the hypolimnion and subsequent mixing (Fig. 5).

This conceptual model coherently accounts for compositional changes of the hypolimnion, namely the dilution of conservative ions (bromide and magnesium) and increases in sodium, chloride and sulfate inventories. Furthermore, the suggested model explains the increase of $\delta^{18}O_{H2O}$ values in the hypolimnion during the Lisan period (Lazar et al., 2014). The model may also account for the observed gypsum supersaturation in pore-fluid resulting from mixing between two gypsum-saturated waters: 1) a concentrated hypolimnion solution that is saturated with respect to gypsum with a relatively high Ca^{2+}/SO_4^{2-} ratio (see Fig. 6), and 2) A sinking diluted epilimnion solution, which attained gypsum saturation due to the dissolution of calcium sulfate minerals on Mt Sedom and characterized by lower ratio Ca^{2+}/SO_4^{2-} ratio. Mixing between two such saturated solutions would result in supersaturation, as demonstrated by the mixing line in Fig. 6.

In order to penetrate Lake Lisan's hypolimnion, any solution dissolving the Sedom diapir would have to flow downwards on the south-west flanks of Lake Lisan and cross the epilimnion–hypolimnion boundary. Such a condition could be met provided the solution density is equal to, or in excess of, the hypolimnion water. Given a density value greater than epilimnion water, but lower than the hypolimnion, any sinking solution would spread at the boundary between the two, being buoyant and forming an intermediate layer of solution. The calculated densities of the hypolimnion are derived from the pore-fluids which roughly lie in a range of 1.20–1.24 kg L^{-1} between ca. 117 to 54ka, and between 1.16 kg L^{-1} to 1.21 kg L^{-1} between ca. 49ka to 16 ka (Levy et al., 2017).

A range of possible compositions for these sinking epilimnic waters were theorized and their densities were estimated. For detailed information on the methods and the results the reader is referred to section 1 and Figs. A1 and A2 in the appendix material. The most concentrated pore-fluid solution found at ca. 117ka was assumed to represent the lake solution prior to the onset of the stratification and dilution that characterized Lake Lisan. Thus, this solution was diluted to factors of 3, 4, 5, and 6 producing possible variations of Lake Lisan epilimnic water. Anhydrite, gypsum and

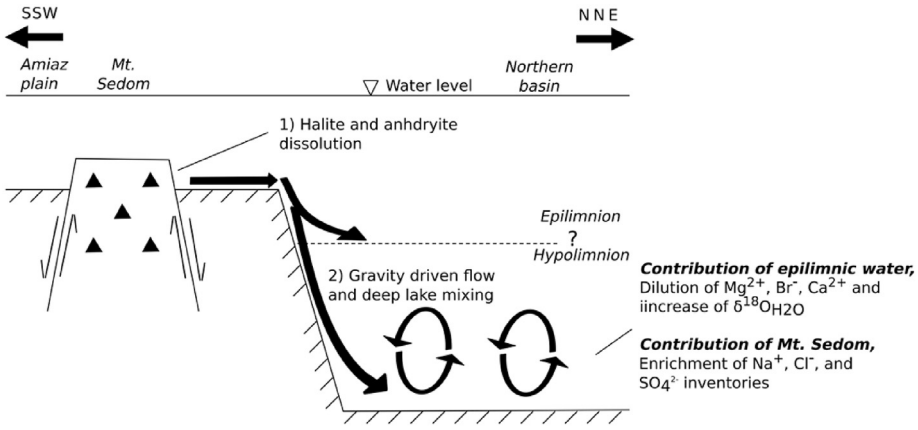

Fig. 5. Schematic presentation of the transport of epilimnion waters and solutes to Lake Lisan's hypolimnion following dissolution of the Sedom salt diapir.

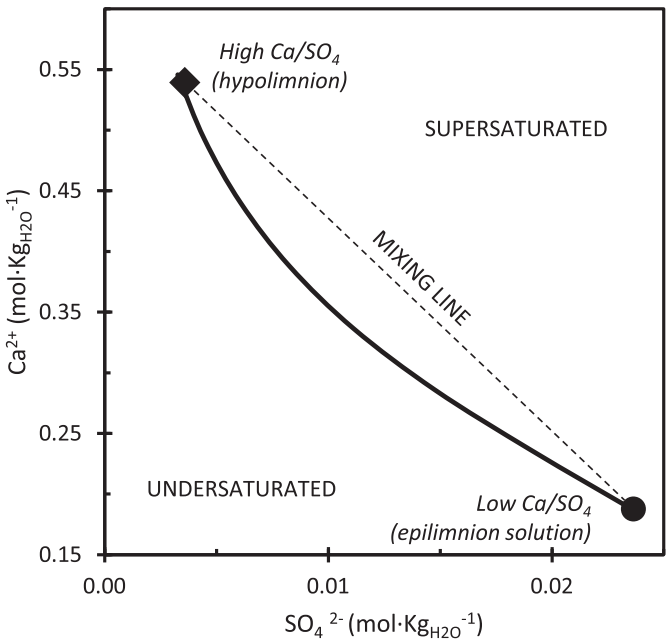

Fig. 6. Schematic gypsum saturation curve (black line) and a mixing line (dotted) between two gypsum saturated end members. End members: calcium rich and sulfate poor solution (high Ca/SO_4; black filled diamond) and a relatively calcium poor and more sulfate rich solution of Ca-Cl composition (low Ca/SO_4; black filled circle). The former represents the Ca-Chloride brine in the hypolimnion at the onset of sulfate accumulation (i.e. pore-fluid composition at 235mblf/ca. 117ka). Note that all mixtures between the two end members are supersaturated with respect to gypsum.

halite were then dissolved into these solutions at various proportions. As outlined below, the proportion and ratio of halite to calcium-sulfate minerals were key parameters for the chemical properties of the solutions. The density of each new solution was then estimated using PHREEQC software.

In the hypersaline modern Dead Sea, gypsum is more soluble than anhydrite, as emphasized by the relative difference in their saturation state: $\Omega_{gypsum} = 1.42$ as opposed to $\Omega_{anhydrite} = 1.94$ (Reznik et al., 2009). However, when the ca. 117ka solution, which is somewhat similar to the modern Dead Sea, was diluted, it was found that anhydrite became more soluble than gypsum (see appendix Fig. A1). Such a trait suggests that diluted Ca-Cl solutions, characteristic of Lake Lisan's epilimnic waters, may have dissolved anhydrite at Mt. Sedom while simultaneously reaching supersaturation with respect to gypsum. These conditions may explain the dual mineral assemblage of anhydrite and gypsum found in the caprock (Zak, 1967). Given the significant abundance of anhydrite on Mt. Sedom in comparison to gypsum, more focus was then given to anhydrite dissolution in the investigation detailed below.

The most dominant parameter affecting solution density was the magnitude of halite dissolution, which can increase solution density to a maximum of ~1.206 kg L^{-1} when halite is dissolved until saturation (*i.e.* $\Omega_{halite} = 1$; see appendix Fig. A1). The solution density value decreases slightly with increasing dilution of the solutions. However, when solutions are saturated to halite, the solubility of anhydrite decreases and less sulfate can be added as a result of anhydrite dissolution. More realistically, anhydrite may have initially been dissolved until saturation, prior to halite, given the setting of the anhydrite caprock in contact with the salt-mirror (Vroman, 1950). Given that the long term sulfate and chloride replenishment ratio in Lake Lisan between ca. 117ka to 20ka, is ~1:70 ($9 \cdot 10^{12}$ mol sulfate: $6.3 \cdot 10^{14}$ mol chloride; section 4.3), anhydrite and halite subsequently dissolved in the solutions at a ratio of ~1:70. If dissolution also takes place at this ratio, anhydrite would reach saturation before attainment of halite saturation. All solutions diluted to the various ratios mentioned above have significantly increased sulfate concentrations (*i.e.* >40 mM) and while they are undersaturated with respect to halite, their densities reach a range around that of pore-fluids corresponding to ca. 49ka to 16 ka (Fig. 7).

Solution temperature may have also played a critical role in the magnitude of anhydrite dissolution, with increasing dissolution facilitated by decreasing temperature. To retain the 1:70 anhydrite to halite ratio, a reduced temperature of solution significantly increases anhydrite dissolution, and thereby enables increased halite dissolution and subsequent solution density. To emphasize this effect, Fig. 7 presents the calculated densities for a range of diluted brines that dissolved anhydrite and halite to the required 1:70 ratio at both 15 °C and 25 °C.

As mentioned, all calculated sulfate concentrations increase to values above 40 mM (Fig. 7) and can explain the observed sulfate increase during the last glacial period reaching a maximum of 33 mM in pore-fluid (Fig. 3). Mixing these solutions back with the original ca. 117ka solution as an analogy for mixing in the hypolimnion, allows the saturation state of gypsum to increase above that of the pore-fluid composition at ca. 20ka (*i.e.* $\Omega_{gypsum} > 3.3$; see appendix Fig. A2).

To summarize, the magnitude of halite dissolution from the Sedom diapir was the dominant factor controlling penetration of

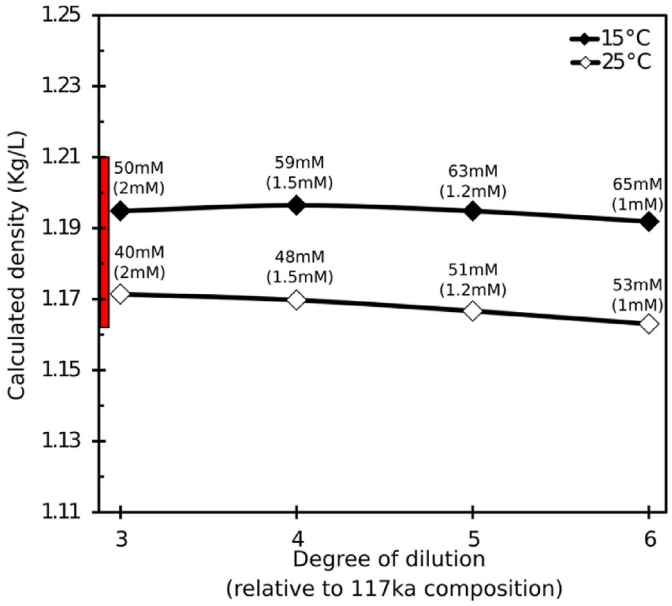

Fig. 7. Solution densities of the ca. 117ka brine diluted to various degrees (representative of epilimnion solution) followed by dissolution of anhydrite and halite. Each data point is a solution which dissolved anhydrite until saturation, followed by halite dissolution at a mole ratio of 1:70. Sulfate concentrations are noted above the data points while the concentrations prior to dissolution are noted in brackets. Calculations are for solutions at 15 °C (filled diamonds) and 25 °C (empty diamonds). The range of pore-fluid calculated densities between ca. 49 to 16ka is shown for comparison (red rectangle). (For interpretation of the references to colour in this figure legend, the reader is referred to the Web version of this article.)

the solution below the epilimnion-hypolimnion interface and subsequent mixing. As dissolution of calcium sulfate minerals is an exothermic reaction, the extent of anhydrite dissolution, which determined the quantity of sulfate added to the solution, increased with decreasing solution temperatures. Indeed the observed increase in sulfate concentrations over the entire glacial period with a maximum for sulfate concentrations (and supersaturation for gypsum) observed in pore-fluids corresponding to the last glacial maximum (LGM), the coldest interval of the last glacial period, is in itself evidence suggesting that cool epilimnion waters of Lake Lisan played a role in facilitating increased anhydrite dissolution during that time.

Between ca. 117ka to 54ka, gravity-driven flow of sinking epilimnion solution due to density differences was mostly limited to reaching the epilimnion/hypolimnion interface, where a significant sulfate-rich buoyant intermediate layer likely formed. Between ca. 49ka to 16ka, when the hypolimnion was characterized by relatively lower solution density in comparison to the preceding time-interval, the solution could have reached the hypolimnion as shown by the conceptual paleo-limnological model (Fig. 5). It is important to stress that over the entire ~100kyr interval the hypolimnion solution changed in composition, suggesting mixing and ongoing increasing hypolimnion volume. As a result, the internal epilimnion-hypolimnion boundary was elevated over time. Together with structural changes and weakening gradient of the chemocline, the kinetic energy provided by the sinking water mass may have enhanced turbulent mixing of solutes in the hypolimnion (Lazar et al., 2014). Given these conditions, a decrease in solution density and total dissolved solids of the hypolimnion solution between ca. 54ka to 49ka may have resulted. However, further investigation of this process requires physical modeling which is beyond the scope of this study.

4.6. Dissolution of anhydrite as a source for Lake Lisan gypsum deposits

As Lake Lisan's hypolimnion was supersaturated with respect to gypsum and rich in sulfate, it may be possible that a large portion of the Lisan water column was similarly supersaturated and sulfate-rich. Indeed, such conditions may be more favorable for precipitation of thick primary gypsum layers such as those observed in the core and exposed sections of the Lisan Fm. at the marginal terraces (Torfstein et al., 2005, 2008; Torfstein and Turchyn, 2017). Gypsum precipitation would have occurred following full or partial water column mixing caused by lake level drops. These drops may have been instigated by periods of less humid conditions, corresponding to Heinrich events as suggested by Stein et al. (1997) and Torfstein et al. (2013).

Here we make a first order estimation whether the sulfate reservoir in Lake Lisan, based on the pore-fluid concentrations, can contribute to forming the thickest gypsum layer found at the top of the Lisan Fm. This Upper Gypsum Unit (UGU) has a maximum net thickness of gypsum of ~85 cm at Masada (Torfstein et al., 2008) and 107 cm in the 5017-1-A core from the deep lake (Torfstein and Turchyn, 2017). Assuming that the water column at ca. 20ka had homogeneous sulfate concentrations of 33 mM, as inferred from pore-fluids, and the excess sulfate above saturation was 21 mM (based on the estimate in section 4.2), precipitation of gypsum to attain saturation would result in the accumulation of 0.00124 m per 1 m of solution (molecular weight of gypsum 136.14 $gr \cdot mol^{-1}$; density of 2310 kg m^{-3}). Multiplying this value by the water column thickness at that time will provide an estimate of gypsum thickness following precipitation.

Estimates of the water level during this period are ~200 m below mean sea level (mbmsl). Assuming ~720mbmsl to the floor of the modern Dead Sea, plus an additional thickness of sediments below of ~106 m, minus 20 m based on a subsidence rate of ~1 m per kyr for the deep lake (Bartov et al., 2006), the depocenter of the lake was around 806mbmsl at ca. 20ka. This suggests a maximum water column thickness ~606 m. Thus, ~75 cm of gypsum could have precipitated to attain saturation with no lake level drop needed, a thickness roughly similar to the net thickness of gypsum at Masada and in the core (Torfstein et al., 2008; Torfstein and Turchyn, 2017).

The gypsum thickness estimate is a first order estimation which ignores changing bathymetry and decreasing thickness of primary gypsum layers in the Lisan Fm. with increasing distance away from the Northern Basin. To calculate the average thickness of gypsum precipitated in the entire Lake Lisan it would be necessary to calculate the average water column depth. This can be estimated by dividing the volume (L^3) by the surface area (L^2) of Lake Lisan. Both lake volume and surface area can be estimated using modern Dead Sea basin hypsometric curves and a lake level of 200mbmsl at ca. 20ka (Hall, 1996). This yields $4.90 \cdot 10^{11}$ m^3 and $2.84 \cdot 10^9$ m^2, for lake volume and lake surface area respectively, and an average water column depth of 173 m. It is important to note that this calculation ignores the volume of accumulated sediments since the late last glacial which would cause the average water column depth value to increase. The average thickness of gypsum spanning across the area covered by Lake Lisan would have been 21 cm after the LGM, given no lake level drop and assuming that the lake carried sulfate concentrations similar to that of the pore-fluid.

4.7. The sulfur system of Lake Lisan

The differences between $\delta^{34}S_{sulfate}$ and $\delta^{18}O_{sulfate}$ of pore-fluid, representative of the hypolimnion solution, and the $\delta^{34}S_{gypsum}$ and $\delta^{18}O_{gypsum}$ of primary gypsum, at corresponding depth intervals in the core, can be used to reconstruct the limnological

structure of the water column. As discussed in the results section, $\delta^{34}S_{sulfate}$ and $\delta^{18}O_{sulfate}$ of pore-fluids show little evidence of active microbial sulfate reduction in their isotope composition. This differs from the $\delta^{34}S_{gypsum}$ and $\delta^{18}O_{gypsum}$ of primary gypsum layers at similar depths which have enriched values (blue triangles in comparison to black diamonds in Fig. 3o and p). Thus, it can be inferred that the contribution of solutes from Mt. Sedom dominated the effects of microbial sulfate reduction at Lake Lisan's hypolimnion floor. A requirement for microbial sulfate reduction is labile organic material: the retention of these high sulfate concentrations may be evidence of limited availability of labile organic material at the lake's floor and in its sediments. Based on these observations we suggest that the active microbial sulfate reduction occurred at intermediate depths in Lake Lisan, possibly within a sulfate rich intermediate layer suggested in the model of section 4.3. This is further supported by the fact that gypsum deposits with enriched ^{34}S and ^{18}O isotope signatures are also found along the marginal terraces, at elevations hundreds of meters above the lake depocenter. An intermediate and anoxic water-layer may have provided a more suitable location for microbial sulfate reduction due to both a lower salinity in comparison to the hypolimnion, along with more accessible access to labile organic material deriving, for example, from freshwater runoff or authigenic organisms in the surface waters and epilimnion.

Modern day analogies where sulfate reduction appears to have occurred in a stratified hypersaline environment, are the anoxic and hypersaline brines found in the Bannock and Tyro basins of the Mediterranean Sea (Vengosh and Starinsky, 1993). It was suggested that enhanced sulfate reduction occurs at the steep chemocline, or the seawater-brine interface (Luther et al., 1990), where particulate organic carbon and dissolved organic carbon concentrations are highest and allow for enhanced bacterial activity (Henneke and De-Lange, 1990). In Lake Lisan, precipitation of the ^{34}S and ^{18}O enriched gypsum would thus occur due to mixing between the aerated epilimnion and a thick sulfate rich anoxic intermediate layer where sulfate reduction was active. Such a process could have been instigated as a result of relatively small lake level drops, or decreasing surface water temperatures (as suggested in this study), which would have caused mixing in the upper and intermediate waters and, in turn, would have pushed gypsum to even higher supersaturation. This mechanism could have allowed for the sulfate reservoir in the lake hypolimnion to maintain its original isotope composition, similar to that of the anhydrite at Mt. Sedom. Only during the deglacial at ca. 17.1 to 15.5ka, when the UGU gypsum precipitated, was there a complete transition from meromictic to holomictic conditions as suggested by Torfstein and Turchyn (2017), which subsequently involved precipitation of the deep hypolimnion sulfate reservoir. This suggestion is supported by the negative trend of $\delta^{34}S_{gypsum}$ and $\delta^{18}O_{gypsum}$ values in the UGU of the Lisan Fm., which converge to $\delta^{34}S_{sulfate}$ and $\delta^{18}O_{sulfate}$ values seen in pore-fluids (Fig. 3o and p at ~100 to ~90mblf).

5. Summary and conclusions

This study presents an investigation of the long-term sulfate reservoir changes in the hypolimnion of Lake Lisan. We analyzed concentrations and stable isotopes in pore-fluids from cores that were drilled at the lake floor by ICDP (International Continental Drilling Programs). The main results and conclusions of the study are:

* Significant amounts of chloride, sodium and sulfate ions were replenished in the lake due to dissolution of halite and anhydrite from the Mt. Sedom salt diapir.
* The dissolution of these evaporitic minerals occurred when the diapir was submerged in the last glacial Lake Lisan. Dissolution was facilitated by diluted and cool epilimnic waters.
* Given the increase in solution density following dissolution, and subsequent gravity driven flow, a buoyant sulfate rich intermediate layer at the epilimnion-hypolimnion boundary was formed and solution also penetrated below into the hypolimnion.
* Following mixing, the hypolimnion became replenished with chloride, sodium and sulfate and supersaturated to gypsum. Hypolimnion volume increased. Other solutes, such as bromide and magnesium, were simultaneously diluted.

The described processes resulted in the transition of the waterbody filling the Dead Sea Basin from a halite-precipitating lake during times of low lake level stands of the last interglacial period, to a gypsum-precipitating lake during the last glacial period. Similar processes may have occurred during former interglacial-glacial cycles during the past 3 million years of lacustrine history at the Dead Sea Basin.

Acknowledgements

We would like to thank both A. Starinsky and an anonymous reviewer for their fruifull and insighful reviews. We thank all who participated in the drilling operations, opening and descriptions of the drilled cores. We sincerely thank I. Swaed from GSI, E. Eliani-Russak, M. Adler, I. Bar-Or, N. Avrahamov, and A. Russak from BGU for taking part in sampling and measuring during the first pore-fluid extration campaign. D. Stiber, G. Sharabi, O. Berlin and other members of the GSI geochemical division carried out major ion analysis. J. Ganor, P. Rendal, and A. Reiss from BGU for the utilities and helping measure sulfate. We thank S. Turchyn for the utilities used in sulfate and gypsum isotope analyses. We thank also N. Amiel and S. Stein for helping in sampling the rock formation of Mt. Sedom. M. Stiller, R. Weinberger, and N. Weber for fruitful discussion and advice. The scientific study was supported by an Excellence Center grant of the Israel Science Foundation (ISF) grant 1736/11 to B.L and a grant of the Ministry of Tourism of Israel.

Appendix A. Supplementary data

Supplementary data to this article can be found online at https://doi.org/10.1016/j.quascirev.2019.105871.

References

Balci, N., Shanks III, W.C., Mayer, B., Mandernack, K.W., 2007. Oxygen and sulfur isotope systematics of sulfate produced by bacterial and abiotic oxidation of pyrite. Geochem. Cosmochim. Acta 71 (15), 3796–3811.
Bartov, Y., Stein, M., Enzel, Y., Agnon, A., Reches, Z.E., 2002. Lake levels and sequence stratigraphy of lake Lisan, the late Pleistocene precursor of the Dead Sea. Quat. Res. 57 (1), 9–21.
Bartov, Y., Agnon, A., Enzel, Y., Stein, M., 2006. Late Quaternary faulting and subsidence in the central Dead Sea basin. Isr. J. Earth Sci. 55 (1).
Begin, Z.B., Erlich, A., Nathan, I., 1974. Lisan lake, the representative of the Pleistocene age in the dead sea. Geol. Surv. Isr. Bull. 63, 1–30.
Belmaker, R., Stein, M., Beer, J., Christl, M., Fink, D., Lazar, B., 2014. Beryllium isotopes as tracers of lake Lisan (last glacial Dead Sea) hydrology and the Laschamp geomagnetic excursion. Earth Planet. Sci. Lett. 400, 233–242.
Bishop, T., Turchyn, A.V., Sivan, O., 2013. Fire and brimstone: the microbially mediated formation of elemental sulfur nodules from an isotope and major element study in the Paleo-Dead Sea. PLoS One 8 (10), e75883.
Böttcher, M.E., Thamdrup, B., 2001. Anaerobic sulfide oxidation and stable isotope fractionation associated with bacterial sulfur disproportionation in the presence of MnO2. Geochem. Cosmochim. Acta 65 (10), 1573–1581.
Böttcher, M.E., Thamdrup, B., Vennemann, T.W., 2001. Oxygen and sulfur isotope fractionation during anaerobic bacterial disproportionation of elemental sulfur. Geochem. Cosmochim. Acta 65 (10), 1601–1609.
Böttcher, M.E., Thamdrup, B., Gehre, M., Theune, A., 2005. 34S/32S and 18O/16O

fractionation during sulfur disproportionation by Desulfobulbus propionicus. Geomicrobiol. J. 22 (5), 219–226.
Calmels, D., Gaillardet, J., Brenot, A., France-Lanord, C., 2007. Sustained sulfide oxidation by physical erosion processes in the Mackenzie River basin: climatic perspectives. Geology 35 (11), 1003–1006.
Coianiz, L., Ben-Avraham, Z., Stein, M., Lazar, M., 2019. Spatial and temporal reconstruction of the late Quaternary Dead Sea sedimentary facies from geophysical properties. J. Appl. Geophys. 160, 15–27.
Gavrieli, I., 1997. Halite deposition in the Dead Sea. In: Niemi, T., Ben-Avraham, Z., Gat, J.R. (Eds.), The Dead Sea , the Lake and its Setting. Oxford University Press, pp. 161–170.
Haase-Schramm, A., Goldstein, S.L., Stein, M., 2004. U-Th dating of Lake Lisan (late Pleistocene Dead Sea) aragonite and implications for glacial East Mediterranean climate change. Geochem. Cosmochim. Acta 68 (5), 985–1005.
Hall, J.K., 1996. Digital topography and bathymetry of the area of the Dead Sea depression. Tectonophysics 266 (1–4), 177–185. https://doi.org/10.1016/S0040-1951(96)00189-8.
Haliva-Cohen, A., Stein, M., Goldstein, S.L., Sandler, A., Starinsky, A., 2012. Sources and transport routes of fine detritus material to the Late Quaternary Dead Sea basin. Quat. Sci. Rev. 50, 55–70.
Henneke, E., De Lange, G.J., 1990. The distribution of DOC and POC in the water column and brines of the Tyro and Bannock basins. Mar. Chem. 31 (1–3), 113–122.
Herut, B., Gavrieli, I., Halicz, L., 1998. Coprecipitation of trace and minor elements in modern authigenic halites from the hypersaline Dead Sea brine. Geochem. Cosmochim. Acta 62 (9), 1587–1598.
Katz, A., Kolodny, Y., Nissenbaum, A., 1977. The geochemical evolution of the Pleistocene Lake Lisan-Dead Sea system. Geochem. Cosmochim. Acta 41 (11), 1609–1626.
Kiro, Y., Goldstein, S.L., García-Veigas, J., Levy, E., Kushnir, Y., Stein, M., Lazar, B., 2017. Relationships between lake-level changes and water and salt budgets in the Dead Sea during extreme aridities in the Eastern Mediterranean. Earth Planet. Sci. Lett. 464, 211–226. https://doi.org/10.1016/j.epsl.2017.01.043.
Kitagawa, H., Stein, M., Goldstein, S.L., Nakamura, T., Lazar, B., 2017. Radiocarbon chronology of the DSDDP core at the deepest floor of the Dead Sea. Radiocarbon 59 (2), 383–394. https://doi.org/10.1017/RDC.2016.120.
Lazar, B., Sivan, O., Yechieli, Y., Levy, E.J., Antler, G., Gavrieli, I., Stein, M., 2014. Long-term freshening of the Dead Sea brine revealed by porewater Cl^- and $\delta^{18}O$ in ICDP Dead Sea deep-drill. Earth Planet. Sci. Lett. 400, 94–101. https://doi.org/10.1016/j.epsl.2014.03.019.
Levy, E.J., Stein, M., Lazar, B., Gavrieli, I., Yechieli, Y., Sivan, O., 2017. Pore-fluids in Dead Sea sediment core reveal linear response of lake chemistry to global climate changes. Geology 45 (4), 315–318. https://doi.org/10.1130/G38685.1.
Levy, E.J., Yechieli, Y., Gavrieli, I., Lazar, B., Kiro, Y., Stein, M., Sivan, O., 2018. Salt precipitation and dissolution in the late Quaternary Dead Sea: evidence from chemical and δ 37 Cl composition of pore-fluids and halites. Earth Planet. Sci. Lett. 487, 127–137.
Luther III, G.W., Catalano, G., De Lange, G.J., Woittiez, J.R.W., 1990. Reduced sulfur in the hypersaline anoxic basins of the Mediterranean Sea. Mar. Chem. 31 (1–3), 137–152.
Neev, D., Emery, K.O., 1967. The Dead Sea, depositional processes and environments of evaporites. Geol. Surv. Isr. Bull. 41, 147.
Neugebauer, I., Brauer, A., Schwab, M.J., Waldmann, N.D., Enzel, Y., Kitagawa, H., Torfstein, A., Frank, U., Dulski, P., Agnon, A., Ariztegui, D., 2014. Lithology of the long sediment record recovered by the ICDP Dead Sea deep drilling Project (DSDDP). Quat. Sci. Rev. 102, 149–165. https://doi.org/10.1016/j.quascirev.2014.08.013.
Nissenbaum, A., Kaplan, I.R., 1976. Sulfur and carbon isotopic evidence for biogeochemical processes in the Dead Sea ecosystem. Environ. Biogeochem. 1, 309–325.
Palchan, D., Erel, Y., Stein, M., 2019. Mobilization of fine detritus to the Dead Sea Basin during the late glacial and early Holocene. Quat. Sci. Rev. 218, 395–405.
Parkhurst, D.L., Appelo, C.A.J., 1999. User's Guide to PHREEQC (Version 2): A Computer Program for Speciation, Batch-Reaction, One-Dimensional Transport, and Inverse Geochemical Calculations.
Pitzer, K.S., 1973. Thermodynamics of electrolytes. I. Theoretical basis and general equations. J. Phys. Chem. 77 (2), 268–277.
Raab, M., Friedman, G.M., Spiro, B., Starinsky, A., Zak, I., 2000. The geological history of Pliocene-Pleistocene evaporites in Mount Sedom (Israel) and how strontium and sulfur isotopes relate to their origin. Carbonates Evaporites 15 (2), 93.
Reznik, I.J., Gavrieli, I., Ganor, J., 2009. Kinetics of gypsum nucleation and crystal growth from Dead Sea brine. Geochem. Cosmochim. Acta 73 (20), 6218–6230.
Starinsky, A., 1974. Relationship between Ca-Chloride Brines and Sedimentary Rocks in Israel. Doctoral dissertation in Hebrew. The Hebrew University of Jerusalem.
Stein, M., Starinsky, A., Katz, A., Goldstein, S.L., Machlus, M., Schramm, A., 1997. Strontium isotopic, chemical, and sedimentological evidence for the evolution of Lake Lisan and the Dead Sea. Geochem. Cosmochim. Acta 61 (18), 3975–3992.
Stein, M., 2001. The sedimentary and geochemical record of Neogene-Quaternary water bodies in the Dead Sea Basin-inferences for the regional paleoclimatic history. J. Paleolimnol. 26 (3), 271–282.
Stein, M., 2014. The evolution of Neogene-Quaternary water-bodies in the Dead Sea rift valley. In: Garfunkel, Z., Ben-Avraham, Z., Kagan, E. (Eds.), Dead Sea Transform Fault System: Reviews. Modern Approaches in Solid Earth Sciences, vol. 6. Springer, Dordrecht.
Stein, M., Goldstein, S., 2017. Lake Lisan. In: Enzel, Y., Bar-Yosef, O. (Eds.), Quaternary of the Levant: Environments, Climate Change, and Humans. Cambridge University Press, Cambridge, pp. 107–114. https://doi.org/10.1017/9781316106754.012.
Steinhorn, I., 1985. The disappearance of the long term meromictic stratification of the Dead Sea. Limnol. Oceanogr. 30, 451–472. https://doi.org/10.4319/lo .1985 .30 .3 .0451.
Stiller, M., Gat, J.R., Kaushansky, P., 1997. Halite precipitation and sediment deposition as measured in sediment traps deployed in the Dead Sea 1981-1983. In: Niemi, T.M., Ben-Avraham, Z., Gat, J.R. (Eds.), The Dead Sea: the Lake and its Setting. Oxford University Press, pp. 171–183.
Thamdrup, B.O., Finster, K., Hansen, J.W., Bak, F., 1993. Bacterial disproportionation of elemental sulfur coupled to chemical reduction of iron or manganese. Appl. Environ. Microbiol. 59 (1), 101–108.
Torfstein, A., Gavrieli, I., Stein, M., 2005. The sources and evolution of sulfur in the hypersaline Lake Lisan (paleo-Dead Sea). Earth Planet. Sci. Lett. 236 (1–2), 61–77.
Torfstein, A., Gavrieli, I., Katz, A., Kolodny, Y., Stein, M., 2008. Gypsum as a monitor of the paleo-limnological–hydrological conditions in lake Lisan and the Dead Sea. Geochem. Cosmochim. Acta 72 (10), 2491–2509.
Torfstein, A., Goldstein, S.L., Stein, M., Enzel, Y., 2013. Impacts of abrupt climate changes in the levant from last glacial Dead Sea levels. Quat. Sci. Rev. 69, 1–7.
Torfstein, A., Goldstein, S.L., Kushnir, Y., Enzel, Y., Haug, G., Stein, M., 2015. Dead Sea drawdown and monsoonal impacts in the Levant during the last interglacial. Earth Planet. Sci. Lett. 412, 235–244. https://doi.org/10.1016/j.epsl.2014.12.013.
Torfstein, A., Turchyn, A.V., 2017. Rates and cycles of microbial sulfate reduction in the hyper-saline Dead Sea over the last 200 kyrs from sedimentary δ34S and δ18O (SO4). Front. Earth Sci. 5, 62.
Vengosh, A., Starinsky, A., 1993. Relics of evaporated sea water in deep basins of the eastern Mediterranean. Mar. Geol. 115 (1–2), 15–19.
Vroman, 1950. The movement and solution of salt bodies as applied to Mount Sdom. Isr. Explor. J. 1 (4), 185–193.
Weber, N., Yechieli, Y., Stein, M., Yokochi, R., Gavrieli, I., Zappala, J., Mueller, P., Lazar, B., 2018. The circulation of the Dead Sea brine in the regional aquifer. Earth Planet. Sci. Lett. 493, 242–261.
Weinberger, R., Agnon, A., Ron, H., 1997. Paleomagnetic reconstruction of a diapir emplacement: a case study from Sedom diapir, the Dead Sea rift. J. Geophys. Res. Solid Earth 102 (B3), 5173–5192.
Weinberger, R., Begin, Z.B., Waldmann, N., Gardosh, M., Baer, G., Frumkin, A., Wdowinski, S., 2006. Quaternary rise of the sedom diapir, Dead Sea basin. Geol. Soc. Am. Spec. Pap. 401, 33–51. https://doi.org/10.1130/2006.2401(03).
Weinberger, R., Bar-Matthews, M., Levi, T., Begin, Z.B., 2007. Late-Pleistocene rise of the Sedom diapir on the backdrop of water-level fluctuations of Lake Lisan, Dead Sea basin. Quat. Int. 175 (1), 53–61. https://doi.org/10.1016/j.quaint.2007.03.007.
Zak, I., 1967. The Geology of Mt. Sedom. Ph. D. thesis. The Hebrew University, Jerusalem (in Hebrew with English abstract).
Zak, I., Bentor, Y.K., 1972. Some new data on the salt deposits of the Dead Sea area, Israel. In: Geology of Saline Deposits: Paris, UNESCO, Proceedings of the Hannover Symposium, pp. 137–146.
Zilberman, T., Gavrieli, I., Yechieli, Y., Gertman, I., Katz, A., 2017. Constraints on evaporation and dilution of terminal, hypersaline lakes under negative water balance: the Dead Sea, Israel. Geochem. Cosmochim. Acta 217, 384–398. https://doi.org/10.1016/j.gca.2017.08.040.